J Sci Comput (2013) 57:349–371
DOI 10.1007/s10915-013-9709-9

Image Restoration via Tight Frame Regularization and Local Constraints

Fang Li · Tieyong Zeng

Received: 29 January 2012 / Revised: 25 March 2013 / Accepted: 26 March 2013 /
Published online: 8 April 2013

Abstract In this paper, we propose two variational image denosing/deblurring models which combine tight frame regularization with two types of existing local constraints. Additive white Gaussian noise is assumed in the models. By Lagrangian multiplier method, the local constraints correspond to the fidelity term with spatial adaptive parameters. As the fidelity parameter is bigger in the image regions with textures than in the cartoon region, our models can recover more texture while denoising/deblurring. Fast numerical schemes are designed for the two models based on split Bregman (SB) technique and doubly augmented Lagrangian (DAL) method with acceleration. In the experiments, we show that the proposed models have better performance compared with the existing total variation based image restoration models with global or local constraints and the frame based model with global constraint.

Keywords Image restoration · Tight frame · Local constraint · Split Bregman · Doubly augmented Lagrangian

1 Introduction

Images are often blurred and corrupted by Gaussian noise during image acquisition and transmission process. In many image processing tasks such as edge detection, segmentation and object recognition, image denoising and deblurring are important preprocessing steps. In the following, we assume that f is a given grayscale image defined on Ω, a bounded, open

This work is supported by the 973 Program (2011CB707104), the National Science Foundation of China (11001082, 11271049), and RGC 203109, 211710, 211911 and RFGs of HKBU.

F. Li
Department of Mathematics, East China Normal University, Shanghai, China

T. Zeng (✉)
Department of Mathematics, Centre for Mathematical Imaging and Vision, Hong Kong Baptist University, Kowloon Tong, Hong Kong
e-mail: zeng@hkbu.edu.hk

rectangular subset of $\mathbb{R}^2$, with Lipschitz boundary. Assume that u is the true image and f is the observed image with blur and Gaussian white noise, that is

$$f = Ku + n.$$

Here the blurring kernel K is a bounded linear operator from $L^2(\Omega)$ to $L^2(\Omega)$, which is assumed to be known. The quantity n denotes white Gaussian noise with zero mean and standard deviation σ. The basic variational model for restoration of image with blur and Gaussian noise is proposed in the seminal work [27,28]. This approach is called ROF model in the later and is described as follows:

$$\begin{cases} \min\limits_{u} \int_{\Omega} |\nabla u| dx \\ s.t., \int_{\Omega} (Ku - f) dx = 0, \int_{\Omega} (Ku - f)^2 dx = \sigma^2 |\Omega|. \end{cases} \tag{1}$$

Here $\int_{\Omega} |\nabla u| dx$ is called total variation (TV) of u which is widely used as regularization term in variational models since it can well preserve edges while smoothing out noise [3]. Through the theoretical analysis in [9], we know that the first mean constraint is automatically satisfied and the second variance constraint is equivalent to:

$$\frac{1}{|\Omega|} \int_{\Omega} (Ku - f)^2 dx \leq \sigma^2. \tag{2}$$

The usual way to solve the ROF model is via the following unconstrained problem:

$$\min_{u \in BV(\Omega)} \int_{\Omega} |\nabla u| dx + \lambda \int_{\Omega} (Ku - f)^2 dx, \tag{3}$$

where the second term is a fidelity term, the given parameter $\lambda > 0$ can be regarded as Lagrange multiplier of the second constraint in ROF model. Evidently, λ plays a very important role by controlling the trade-off of regularization and fidelity. If λ is set to be large, then cartoon regions are well denoised while highly textured regions will loose a great part of its information. On the contrary, if λ is set to be too small, texture will be kept but noise will remain in the cartoon regions. Hence a global constraint and thus a global fidelity parameter λ can not produce satisfactory results simultaneously in different image regions. Therefore a variable fidelity parameter which is relatively small in cartoon regions and big in texture regions is favored. Based on this idea, local constraints are proposed to incorporate total variation regularization [2,4,13,17,20,22,27,31].

The use of local constraints on different regions of image was initially proposed in [27] without details. In [4], the authors used a set of local constraints to adapt different regions of the image. They firstly partitioned the image into r regions $O_1, \ldots, O_r$ by some segmentation method and wrote the model as:

$$\begin{cases} \min\limits_{u} \int_{\Omega} |\nabla u| dx \\ s.t., \frac{1}{|O_i|} \int_{O_i} (Ku - f)^2 dx \leq \sigma^2. \end{cases} \tag{4}$$

The corresponding unconstrained formulation is then:

$$\min_{u} \int_{\Omega} |\nabla u| dx + \sum_{i=1}^{r} \frac{\lambda_i}{2} \frac{1}{|O_i|} \left(\int_{O_i} (Ku - f)^2 dx - \sigma^2 \right),$$

where $\{\lambda_i\}_{i=1}^r$ is the Kuhn–Tucker vector (Lagrange multipliers) associated to the constraints in (4) and can be solved with Uzawa's method [15]. This idea is generalized in [2] by replacing the family of constraints in (4) as local constraints of variance:

$$h * (Ku - f)^2 (x) - \sigma^2 \leq 0, \forall x \in \Omega, \tag{5}$$

where $h \geq 0$ is a convolution kernel. By proximal point algorithm [26], the problem is transformed into:

$$\min_u \max_{\lambda \geq 0} \int_\Omega \sqrt{|\nabla u| + \beta^2} + \gamma (u - u^n)^2 + \lambda(x) \left(h * (Ku - f)^2 (x) - \sigma^2\right) dx,$$

where u^n is the value of u in the last iteration. The u subproblem is solved by Chambolle's projection method [8] and the iteration scheme of $\lambda(x)$ follows Uzawa algorithm as:

$$\lambda(x) = \max \left\{\lambda(x) + \rho \left(h * (Ku - f)^2 (x) - \sigma^2\right), 0\right\},$$

where $\rho > 0$ is the step size. We remark that in [17], to solve the local constraints model for denoising, the authors proposed to use gradient descent method and derived an updating formula of $\lambda(x)$ from the Euler–Lagrange equation. This method is generalized to multiplicative noise case in [22]. In [20], the total variation model with expected value constraints is studied. In Gaussian noise case, the constraints are:

$$S(u)(x) := \int_\Omega w(x, y)|Ku - f|(y)dy \leq \sigma, \forall x \in \Omega,$$

where w is the kernel of mean filter. By penalty method, they derived the updating formula of Lagrange multipliers $\lambda(x)$ as:

$$\lambda(x) = \int_\Omega w(x, y) \left(\lambda(y) + \rho \max\{S(u)(y) - \sigma, 0\}\right) dy.$$

In a similar way, the spatially adapted total variation model with L^2 local constraints was studied in [13]. Primal-dual type method and semismooth Newton algorithm were used in the numerical implementation in both [20] and [13], however, they solved not the original problems but some regularized versions.

In the above methods, the local constraints are assumed in the space domain. Another approach is considering the local constraints in the transform domain. In [25], the following model was proposed:

$$\begin{cases} \min_u \int_\Omega |\nabla u| dx \\ s.t., \|Ku - f\|_{\mathcal{D},\infty} \leq \tau, \end{cases} \tag{6}$$

where $\mathcal{D}$ is a dictionary containing finite basis $\{\Psi_i\}_{i=1}^n$, the parameter $\tau > 0$ is depend on the noise level and $\|u\|_{\mathcal{D},\infty} = \sup_{\Psi_i \in \mathcal{D}} |\langle u, \Psi_i \rangle|$. In [34], a theoretical result of this model suggests that the dictionary must represent sparsely the curvatures of solution image in order to obtain a better denoising performance. Moreover, the above model was transformed into the following form in [23]:

$$\begin{cases} \min_u \int_\Omega \sqrt{|\nabla u|^2 + \beta^2} + \beta \langle u, 1 \rangle dx \\ s.t., \pm \langle Ku - f, \Psi_i \rangle - \tau \leq 0. \end{cases} \tag{7}$$

Remark that the constraints in (6) and (7) are equal. Compared with (6), total variation term is replaced by new terms in (7) in order to make the functional satisfy coercivity theoretically. However, the Uzawa algorithm adopted there seems not stable. To tackle this problem, a stable algorithm based on Chambolle-Pock's primal-dual method [10] is proposed [24].

It is well known that one drawback of TV based method is the staircase effects which seems unsatisfactory and brings false edges. The other drawback is the over smoothing of textures. As we know, tight frame has been proved to be a better regularization technique than TV in terms of texture preserving. To overcome the drawbacks of TV regularization and further enhance image quality, in this paper, we propose two novel models combining tight frame regularization with two types of existing local constraints. In one model, we use local variance constraints as in (2). While in the other model, we use linear constraints on the coefficients of dictionary decomposition as in (7). Then fast numerical schemes are designed for both models by taking use of split Bregman (SB) technique [18] and the doubly augmented Lagrangian algorithm (DAL) in [21]. The different formulation of the proposed models and algorithms are based on large amounts of experiments which seem to be the best among many schemes we tested. The difference between our methods with the previous works [2,13,20,23,25] are clear. Firstly, the tight frame regularization is used in stead of TV. Secondly, the numerical algorithms are new since SB and DAL have not been used in the previous works. Thirdly, the numerical results show that the proposed algorithms have higher performance than TV based methods.

The remaining part of this paper is organized as follows. In Sect. 2, we briefly introduce the tight frame, the SB algorithm and the DAL algorithm. Then we propose our Model 1 and Model 2 in Sect. 3. In Sect. 4, we present numerical schemes for both models. Then the numerical simulation examples are given in Sect. 5, which demonstrate that higher performance can be achieved by tight frame regularization than total variation regularization. Finally we conclude our paper in Sect. 6.

2 Mathematical Preliminaries

2.1 Tight Frame and Framelet

In this subsection, we give a brief introduction of tight frame and framelet. The tight frame is widely studied as a regularization method in image restoration problems [5–7]. More details about tight frame can be found in the book [11] and the reference therein. A countable set $X \subset L^2(\mathbb{R})$ is called a tight frame if:

$$\sum_{h\in X} |\langle v, h\rangle|^2 = \|v\|_2^2, \tag{8}$$

holds for all $v \in L^2(\mathbb{R})$, where $\langle\cdot,\cdot\rangle$ is the inner product in $L^2(\mathbb{R})$. For given $\Psi := \{\psi_1, \ldots, \psi_r\} \subset L^2(\mathbb{R})$, define the affine system by dilations and shifts of Ψ as:

$$X(\Psi) := \{\psi_{\ell,j,k} : 1 \le \ell \le r;\, j,k \in \mathbb{Z}\} \quad \text{with} \quad \psi_{\ell,j,k} := 2^{j/2}\psi_l(2^j \cdot -k).$$

When $X(\Psi)$ forms a tight frame of $L^2(\mathbb{R})$, each function ψ_ℓ, $\ell = 1, \ldots, r$, is called a (tight) framelet and the whole system $X(\Psi)$ is called tight wavelet frame.

To construct compactly supported framelet systems, one starts with a compactly supported refinable function $\phi \in L^2(\mathbb{R})$ with a refinement mask (low-pass filter) h_0 such that ϕ satisfies the refinement equation:

$$\widehat{\phi}(2\cdot) = \widehat{h}_0\widehat{\phi}.$$

Here $\widehat{\phi}$ is the Fourier transform of ϕ and $\widehat{h}_0$ is the a trigonometric polynomial with $\widehat{h}_0(0) = 1$. The construction of a tight framelet system is to find a finite set Ψ that satisfies:

$$\widehat{\psi}_\ell(2\cdot) = \widehat{h}_\ell\widehat{\phi},$$

in the fourier domain for some 2π-periodic $\widehat{h}_\ell$. According to the unitary extension principle (UEP), $X(\Psi)$ forms a tight frame provided that the masks $\widehat{h}_\ell$, $\ell = 0, \ldots, r$ satisfy:

$$\sum_{\ell=0}^{r} \widehat{h}_\ell(\eta)\overline{\widehat{h}_\ell(\eta + p\pi)} = \delta_{p,0}, \quad p = 0, 1,$$

for almost all $\eta \in \mathbb{R}$. Moreover, h_ℓ, $\ell = 1, \ldots, r$ corresponds to high pass filters.

In this paper, we adopt the piecewise linear B-spline frame which is widely and successfully used in tight frame based image restoration, image inpainting and image segmentation. It is generated by one low pass filter h_0 and two high pass filters h_1, h_2 which are:

$$h_0 = \frac{1}{4}[1, 2, 1], \ h_1 = \frac{\sqrt{2}}{4}[1, 0, -1], \ h_2 = \frac{1}{4}[-1, 2, -1].$$

After tensor product, we can get the 2D framelet system generated by one low pass filter $H_0 = h_0 \otimes h_0$ and eight high pass filters $H_1 = h_0^T \otimes h_1$, $H_2 = h_0^T \otimes h_2$, $H_3 = h_1^T \otimes h_0$, $H_4 = h_1^T \otimes h_1$, $H_5 = h_1^T \otimes h_2$, $H_6 = h_2^T \otimes h_0$, $H_7 = h_2^T \otimes h_1$, $H_8 = h_2^T \otimes h_2$. Assume H_0 corresponds to the scaling function ϕ and $H_1, \ldots, H_8$ corresponds to framelets $\psi_1, \ldots, \psi_8$. For a given function $f \in L^2(\mathbb{R}^2)$, the L level framelet decomposition of f is the set of coefficients:

$$\left\{\langle f, 2^{-L/2}\phi(2^{-L}\cdot - j)\rangle, \langle f, 2^{-l/2}\psi_i(2^{-l}\cdot - j)\rangle, 1 \le i \le 8, 0 \le l \le L\right\}.$$

In the continuous setting, we use W and W^T to represent the framelet decomposition and reconstruction operator. In the discrete setting, a 2D image of size $m \times n$ can be represented as a vector in $\mathbb{R}^N$ with $N = mn$. We can represent the framelet decomposition and reconstruction as matrix multiplications Wu and $W^T v$ respectively. Let W_0 be the submatrix of W that corresponds to the decomposition with respect to the refinable function, and $W_{l,i}$ the submatrix of W that corresponds to the decomposition at the lth level with respect to the i-th framelet. With this notation, the matrix $W^{(8L+1)N\times N}$ can be written as:

$$W = \begin{pmatrix} W_0 \\ (W_{l,i}) \end{pmatrix} = \begin{pmatrix} W_0 \\ W_{1,1} \\ W_{1,2} \\ \vdots \\ W_{L,8} \end{pmatrix}.$$

By unitary extension principle (UEP), $W^T W = I$, *i.e.*, $u = W^T W u, \forall u \in \mathbb{R}^N$.

2.2 Split Bregman and Augmented Lagrangian Methods

For the general minimization problem:

$$\min_u \|\Phi(u)\|_1 + H(u),$$

where $H(u)$ is convex, we first transform it into a constrained form:

$$\min_{u,d} \|d\|_1 + H(u) \;\; s.t., \;\; \Phi(u) = d. \tag{9}$$

Then the SB algorithm [18] to solve this problem is given by the following iteration scheme:

$$\begin{cases} (u^{k+1}, d^{k+1}) = \arg\min_{u,d} \|d\|_1 + H(u) + \frac{\gamma}{2}\|\Phi(u) - d + b^k\|_2^2, \\ b^{k+1} = b^k + \Phi(u^{k+1}) - d^{k+1}. \end{cases} \tag{10}$$

When using augmented Lagrangian (AL) method to solve problem (9), we first rewrite it as saddle-point problem:

$$\min_{u,d} \max_{v} \|d\|_1 + H(u) + \langle v, \Phi(u) - d\rangle + \frac{\gamma}{2}\|\Phi(u) - d\|_2^2, \tag{11}$$

where v is the Lagrangian multipliers, $\gamma > 0$ is a parameter. The iteration scheme is:

$$\begin{cases} (u^{k+1}, d^{k+1}) = \arg\min_{u,d} \|d\|_1 + H(u) + \langle v^k, \Phi(u) - d\rangle + \frac{\gamma}{2}\|\Phi(u) - d\|_2^2, \\ v^{k+1} = v^k + \delta\left(\Phi(u^{k+1}) - d^{k+1}\right), \end{cases} \tag{12}$$

where $\delta > 0$ is a step size. The first subproblem can be also rewritten as:

$$(u^{k+1}, d^{k+1}) = \arg\min_{u,d} \|d\|_1 + H(u) + \frac{\gamma}{2}\|\Phi(u) - d - \frac{v^k}{\gamma}\|_2^2.$$

Let $\delta = \gamma$ and $b^k = \frac{v^k}{\gamma}$, we obtain the equivalence of SB algorithm in (10) and AL algorithm in (12). SB and AL methods have been widely used in solving image processing problems [1,19,30,32,33].

Furthermore, the first subproblem in (9) can be solved by alternating minimization scheme with one iteration which gives the alternating split Bregman (ASB) algorithm:

$$\begin{cases} u^{k+1} = \arg\min_{u} \|d^k\|_1 + H(u) + \frac{\gamma}{2}\|d^k - \Phi(u) - b^k\|_2^2, \\ d^{k+1} = \arg\min_{d} \|d\|_1 + H(u^{k+1}) + \frac{\gamma}{2}\|d - \Phi(u^{k+1}) - b^k\|_2^2, \\ b^{k+1} = b^k + \Phi(u^{k+1}) - d^{k+1}. \end{cases}$$

Similarly, the ASB algorithm is equivalent to the alternating direction method of multipliers (ADMM) algorithm [16], see [14,29] for details.

2.3 Doubly Augmented Lagrangian Method

Although the convergence of ASB as well as the ADMM method has been extensively studied for convex problems, we can only guarantee the convergence of the dual variable (b^k) but not the primal variables (u^k, d^k). This is one of the motivations of the introduction of the DAL method [21] which has a comprehensive convergence analysis. In the DAL method, the problem (9) is transformed into a saddle-point problem:

$$\min_{u,d} \max_{v} \left\{\|d\|_1 + H(u) + \langle v, \Phi(u) - d\rangle + \frac{\gamma}{2}\|d - \Phi(u)\|_2^2 + \frac{\eta_1}{2}\|u - \bar{u}\|_2^2 + \frac{\eta_2}{2}\|d - \bar{d}\|_2^2\right\},$$

with parameters $\gamma, \eta_1, \eta_2 > 0$. The iteration scheme is given by:

$$\begin{cases} (u^{k+1}, d^{k+1}) = \arg\min_{u,d} \|d\|_1 + H(u) + \frac{\gamma}{2}\|d - \Phi(u) - b^k\|_2^2 + \frac{\eta_1}{2}\|u - \bar{u}\|_2^2 + \frac{\eta_2}{2}\|d - \bar{d}\|_2^2, \\ b^{k+1} = b^k + \left(\Phi(u^{k+1}) - d^{k+1}\right), \end{cases}$$

where $\bar{u}$ and $\bar{d}$ can be taken as u^k and d^k or other forms. The relation of b and v are as in Sect. 2.2. We remark that the DAL method is used to solve image restoration model effectively with l_0 norm regularization in [12].

3 The Proposed Models

In this paper, we focus on texture image restoration. Based on the literatures [5–7,11] and the experiments therein, we know that frame based regularization techniques is very efficient in image processing problems such as image denoising, image debluring and image inpainting et al. Meanwhile, as is studied in Sect. 1, model with local constraints seems better than global constraint in preserving textures while smoothing. Hence, in order to better recovering textures, we propose two models based on tight frame regularization and two types of existing local constraints for image restoration. In the following, we assume K is the blur operator for image deblurring problem and $K = I$ for image denoising problems such that we can unify the formulas.

Assume W is decomposition operator of tight frame as in Sect. 2.1. Our first Model 1 is minimizing the L^1 norm of frame coefficients with local variance constraints:

$$\text{Model 1:} \quad \begin{cases} \min\limits_{u} \|Wu\|_1 \\ s.t., h * (Ku - f)^2(x) - \bar{\sigma}^2 \leq 0. \end{cases} \tag{13}$$

Here the parameter $\bar{\sigma} > 0$ is depend on the noise level and h is a nonnegative normalized convolution kernel such as Gaussian filter or mean filter. When h is mean filter, the constraint just requires that the local variance of noise $n = f - Ku$ at a window centered at x should be less than $\bar{\sigma}^2$. We remark that local variance is a descriptor of texture. The local variance is bigger in the texture region than in the cartoon region.

Assume that D is the decomposition operator corresponding to some dictionary $\mathcal{D}$ with finite basis $\{\Psi_i\}_{i=1}^n \in L^2(\Omega)$. That means, for a function g, $D(g) = \{\langle g, \Psi_i \rangle\}_{i=1}^n$ denotes all the representation coefficients of g using the basis in $\mathcal{D}$. With operator $\mathcal{D}$, we can rewrite the constraints in (7) as

$$\pm D(Ku - f)(\omega) - \tau \leq 0,$$

where ω is the coordinate in the transform domain of operator D. Then we propose the second model as:

$$\text{Model 2:} \quad \begin{cases} \min\limits_{u} \|Wu\|_1 + \frac{\mu}{2}\|Ku - f\|_2^2 \\ s.t., \pm D(Ku - f)(\omega) - \tau \leq 0, \end{cases} \tag{14}$$

where the parameter $\tau > 0$ is dependent on the noise level. Comparing with model (6), we use tight frame regularization to replace the total variation regularization. Moreover, we use an additional term $\frac{\mu}{2}\|Ku - f\|_2^2$ since it has contribution on numerical stability as suggested in [24].

4 Numerical Algorithms

In this section, we derive effective algorithms for the proposed models. Generally speaking, if the algorithm for deblurring problem is established, one can get the algorithm for image denoising by setting $K = I$ directly. It is the case for Model 2. However, for Model 1, we have

more effective algorithm for image denoising than getting by this way. So we will address the algorithms of Model 1 for image denosing and deblurring problems respectively.

4.1 Algorithm of Model 1: Denoising Case

Following the framework of SB method reviewed in Sect. 2, we first rewrite Model 1 ($K = I$) as:

$$\begin{cases} \min\limits_{u} \|d\|_1 \\ s.t., Wu = d,\ h * (u - f)^2 - \bar{\sigma}^2 \le 0. \end{cases} \tag{15}$$

Using AL method to handle the first equality constraints and the general Lagrangian method to handle the inequality constraints, we get the corresponding saddle-point problem of (15):

$$\min_{u,d}\max_{\lambda\ge 0,v}\left\{\|d\|_1 + \langle v, Wu - d\rangle + \frac{\gamma}{2}\|Wu - d\|_2^2 + \langle \lambda, h * (u - f)^2 - \bar{\sigma}^2\rangle\right\}. \tag{16}$$

By the equivalence of SB and AL described at Sect. 2.2, we get the following iteration scheme to solve the above saddle-point problem (16):

$$\begin{cases} (u^{k+1}, d^{k+1}, \lambda^{k+1}) = \arg\min\limits_{u,d}\max\limits_{\lambda\ge 0} \|d\|_1 + \frac{\gamma}{2}\|Wu - d + b^k\|_2^2 + \langle \lambda, h * (u - f)^2 - \bar{\sigma}^2\rangle, \\ b^{k+1} = b^k + Wu^{k+1} - d^{k+1}. \end{cases}$$

In the first subproblem, by a standard calculation, we get that the closed-form solution of d^{k+1} is given by soft shrinkage:

$$d^{k+1} = \text{shrink}\left(Wu^k + b^k, \frac{1}{\gamma}\right),$$

where

$$\text{shrink}(x, c) = \text{sign}(c)\cdot\max\{|x| - c, 0\}.$$

Meanwhile, the first order optimal condition of u is:

$$\gamma W^T(Wu - d^k + b^k) + \bar{\lambda}(u - f) = 0,$$

where $\bar{\lambda} = h * \lambda$. Hence the closed form solution of u is:

$$u^{k+1} = \left(\gamma + \bar{\lambda}\right)^{-1}\left(W^T(d^k - b^k) + \bar{\lambda} f\right).$$

To solve Lagrangian multipliers λ, we use the following iteration scheme:

$$\lambda^{k+1} = \lambda^k + \rho\max\{h * (u^{k+1} - f)^2 - \bar{\sigma}^2, 0\}.$$

Remark that this updating scheme of λ is via gradient ascend method. It is similar to the updating formula in [13] which can be derived by penalty method. Denote the noise residue $n = u^{k+1} - f$. Then $h * (n^2)$ is the local variance of noise. If this variance is smaller than the pre-estimated noise level $\bar{\sigma}$ which indicates cartoon regions, λ remains unchanged. And if the variance is bigger than $\bar{\sigma}$ which indicates some textures in that region, λ becomes larger, more fidelity and less smoothness is favored, thus the textures can be better preserved.

As a summary, we give the algorithm details of Model 1 in Algorithm 1′. Here and in the later we denote $\mathbf{c}$ as a constant matrix whose element is c everywhere and the size is the same as the size of f.

Algorithm 1′ Algorithm of Model 1: Denoising Case

- Initialization: $u^0 = f, b^0 = W\mathbf{0}, d^0 = Wf, \lambda^0 = \mathbf{0}$.
- For $k = 0, 1, 2, \ldots$, repeat until a stopping criterion is reached

$$\begin{aligned} u^{k+1} &= (\gamma + \bar{\lambda})^{-1}\left(\gamma W^T(d^k - b^k) + \bar{\lambda} f\right), \\ d^{k+1} &= \text{shrink}\left(Wu^k + b^k, \gamma^{-1}\right), \\ b^{k+1} &= b^k + Wu^{k+1} - d^{k+1}, \\ \lambda^{k+1} &= \lambda^k + \rho \max\{h * (u^{k+1} - f)^2 - \bar{\sigma}^2, 0\}. \end{aligned}$$

- Output: u^{k+1}.

4.2 Algorithm of Model 1: Deblurring Case

Following the framework of SB method, we first rewrite Model 1 as:

$$\begin{cases} \min\limits_{u} \|d\|_1 \\ s.t., Wu = d, Ku = s, \ h * (s - f)^2 - \bar{\sigma}^2 \le 0. \end{cases} \tag{17}$$

Using AL method to handle the first two equality constraints and the general Lagrangian method to handle the inequality constraints, we get the saddle-point problem of (17) as:

$$\min_{u,d,s} \max_{\lambda \ge 0, v, w} \left\{ \begin{array}{l} \|d\|_1 + \langle v, Wu - d\rangle + \frac{\gamma_1}{2}\|Wu - d\|_2^2 + \langle w, Ku - s\rangle \\ +\frac{\gamma_2}{2}\|Ku - s\|_2^2 + \langle \lambda, h * (s - f)^2 - \bar{\sigma}^2\rangle. \end{array} \right\} \tag{18}$$

where v, w are the Lagrangian multipliers, $\gamma_1, \gamma_2 > 0$ are a parameters. By the equivalence of SB and AL, we get the following iteration scheme to solve the saddle-point problem (18):

$$\begin{cases} (u^{k+1}, d^{k+1}, s^{k+1}) = \arg\min\limits_{u,d,s} \mathcal{E}(u, d, s, b_1^k, b_2^k), \\ b_1^{k+1} = b_1^k + Wu^{k+1} - d^{k+1}, \\ b_2^{k+1} = b_2^k + Ku^{k+1} - s^{k+1}, \\ \lambda^{k+1} = \lambda^k + \rho \max\{h * (s^{k+1} - f)^2 - \bar{\sigma}^2, 0\}, \end{cases}$$

where

$$\mathcal{E}(u, d, s, b_1^k, b_2^k) = \left\{ \begin{array}{c} \|d\|_1 + \frac{\gamma_1}{2}\|Wu - d + b_1^k\|_2^2 + \frac{\gamma_2}{2}\|Ku - s + b_2^k\|_2^2 \\ +\langle \lambda, h * (s - f)^2 - \bar{\sigma}^2\rangle. \end{array} \right\}$$

We will solve the first subproblem in the above saddle-point problem by alternating minimization method. The first order optimal condition of u and s are given by:

$$\begin{aligned} &\gamma_1 W^T(Wu - d + b_1^k) + \gamma_2 K^T(Ku - s + b_2^k) = 0, \\ &\gamma_2(s - Ku - b_2^k) + \bar{\lambda}(s - f) = 0, \end{aligned}$$

where $\bar{\lambda} = h * \lambda$ and K^T denotes the conjugate operator of K. Hence we can get the closed form solutions of u and s:

$$\begin{aligned} u &= \left(1 + K^T K\right)^{-1}\left(W^T(d - b_1^k) + K^T(s - b_2^k)\right), \\ s &= \frac{\gamma_2(Ku + b_2^k) + \bar{\lambda} f}{\gamma_2 + \bar{\lambda}}, \end{aligned}$$

where I denotes the identity matrix. Meanwhile the closed-form solution of d is soft shrinkage as in denoising case:

$$d = \text{shrink}\left(Wu + b_1^k, \frac{1}{\gamma_1}\right).$$

As a summary, we give the algorithm details of Model 1 for image deblurring in Algorithm $1''$.

Algorithm $1''$ Algorithm of Model 1: Deblurring Case

- Initialization: $u^0 = f, b_1^0 = W\mathbf{0}, d_1^0 = Wf, b_2^0 = \mathbf{0}, d_2^0 = Kf, \lambda^0 = \mathbf{c}$.
- For $k = 0, 1, 2, \ldots$, repeat until a stopping criterion is reached

$$\begin{aligned}
u^{k+1} &= \left(\gamma_1 I + \gamma_2 K^T K\right)^{-1}\left(\gamma_1 W^T(d^k - b_1^k) + \gamma_2 K^T(s^k - b_2^k)\right)\\
d^{k+1} &= \text{shrink}\left(Wu^k + b_1^k, \gamma_1^{-1}\right),\\
s^{k+1} &= \frac{\gamma_2(Ku^{k+1} + b_2^k) + \bar{\lambda}^k f}{\gamma_2 + \bar{\lambda}^k}\\
b_1^{k+1} &= b_1^k + Wu^{k+1} - d^{k+1},\\
b_2^{k+1} &= b_2^k + Ku^{k+1} - s^{k+1},\\
\lambda^{k+1} &= \lambda^k + \rho \max\left\{h * (s^{k+1} - f)^2 - \bar{\sigma}^2, 0\right\}.
\end{aligned}$$

- Output: u^{k+1}.

4.3 Algorithm of Model 2

For Model 2, we use DAL method to derive the numerical algorithm. Using DAL on problem (14), we get the following equivalent saddle-point problem:

$$\min_{u,d}\max_{\lambda_\pm \geq 0, v}\left\{\begin{array}{l}\|d\|_1 + \frac{\mu}{2}\|Ku - f\|_2^2 + \langle v, Wu - d\rangle + \frac{\gamma}{2}\|Wu - d\|_2^2\\ +\langle \lambda_+, D(Ku - f) - \tau\rangle + \langle \lambda_-, -D(Ku - f) - \tau\rangle\\ +\frac{1}{2t_u}\|u - \bar{u}\|_2^2 + \frac{1}{2t_d}\|d - \bar{d}\|_2^2 - \frac{1}{2t_\lambda}\|\lambda_+ - \bar{\lambda}_+\|_2^2 - \frac{1}{2t_\lambda}\|\lambda_- - \bar{\lambda}_-\|_2^2.\end{array}\right\} \quad (19)$$

where $\gamma, t_u, t_d, t_\lambda$ are positive parameters. Remark that the proximal terms (the last line of (19)) on primal variables (u, d) are positive which corresponding to minimization problems. On the other hand the proximal term on dual variables (λ_+, λ_-) are negative which corresponding to maximization problems.

Similar as the derivation of SB and AL, we get the following iteration scheme to solve the saddle-point problem (19):

$$\left\{\begin{array}{l}(u^{k+1}, d^{k+1}, \lambda_+^{k+1}, \lambda_-^{k+1}) = \arg\min_{u,d}\max_{\lambda_\pm \geq 0}\mathcal{L}(u, d, \lambda_+, \lambda_-, u^k, d^k, \lambda_+^k, \lambda_-^k),\\ b^{k+1} = b^k + Wu^{k+1} - d^{k+1},\end{array}\right. \quad (20)$$

where

$$\begin{aligned}
&\mathcal{L}(u, d, \lambda_+, \lambda_-, u^k, d^k, \lambda_+^k, \lambda_-^k)\\
&= \|d\|_1 + \frac{\mu}{2}\|Ku - f\|_2^2 + \frac{\gamma}{2}\|Wu - d + b^k\|_2^2
\end{aligned}$$

$$+\langle\lambda_+, D(Ku-f)-\tau\rangle+\langle\lambda_-, -D(Ku-f)-\tau\rangle$$
$$+\frac{1}{2t_u}\|u-u^k\|_2^2+\frac{1}{2t_d}\|d-d^k\|_2^2-\frac{1}{2t_\lambda}\|\lambda_+-\lambda_+^k\|_2^2-\frac{1}{2t_\lambda}\|\lambda_--\lambda_-^k\|_2^2.$$

Then we use alternating minimization method to solve the saddle-point problem in (20). To solve d, we first write the subproblem of d as:

$$\min_d \|d\|_1+\frac{\gamma}{2}\left\|Wu-d+b^k\right\|_2^2+\frac{1}{2t_d}\left\|d-d^k\right\|_2^2. \tag{21}$$

It is equivalent to:

$$\min_d \|d\|_1+\frac{\gamma+t_d^{-1}}{2}\left\|d-\frac{\left(\gamma(Wu+b^k)+t_d^{-1}d^k\right)}{\gamma+t_d^{-1}}\right\|_2^2. \tag{22}$$

Following a standard derivation, we get that d has closed-form solution given by shrinkage operator:

$$d=\text{shrink}\left(\frac{\left(\gamma(Wu+b^k)+t_d^{-1}d^k\right)}{\gamma+t_d^{-1}},\frac{1}{\gamma+t_d^{-1}}\right).$$

Meanwhile, the first order optimal conditions of u, λ_+, λ_- are:

$$\frac{\partial\mathcal{L}}{\partial u}=\mu K^T(Ku-f)+\gamma W^T(Wu-d+b^k)+K^TD^T(\lambda_+-\lambda_-)+\frac{1}{t_u}(u-u^k)=0,$$
$$\frac{\partial\mathcal{L}}{\partial\lambda_+}=D(Ku-f)-\tau-\frac{1}{t_\lambda}(\lambda_+-\lambda_+^k)=0,$$
$$\frac{\partial\mathcal{L}}{\partial\lambda_+}=-D(Ku-f)-\tau-\frac{1}{t_\lambda}(\lambda_--\lambda_-^k)=0.$$

Since the nonnegative constraints on $\lambda_\pm$ is convex, we can derive that the closed-form solutions of u, λ_+, λ_- are:

$$u=\left(\mu t_uK^TK+(1+\gamma t_u)I\right)^{-1}\begin{pmatrix}u^k+\mu t_uK^Tf+\gamma t_uW^T(d-b^k)\\-t_uK^TD^T(\lambda_+-\lambda_-)\end{pmatrix},$$
$$\lambda_+=\max\{\lambda_+^k+t_\lambda(D(Ku-f)-\tau),0\},$$
$$\lambda_-=\max\{\lambda_-^k+t_\lambda(-D(Ku-f)-\tau),0\}.$$

Let

$$G=u^k+\mu t_uK^Tf+\gamma t_uW^T(d^{k+1}-b^k)-t_uK^TD^T(\lambda_+^{k+1}-\lambda_-^{k+1}).$$

Then we can summarize algorithm details of Model 2 in Algorithm 2.

We remark that to accelerate the algorithm, we follow the idea of primal-dual method in [10] and [24] by adding the last updating formula of $\bar{u}$ in the last line of Algorithm 2. At the same time in the iteration formula of $d^{k+1}, b^{k+1}, \lambda_+^{k+1}, \lambda_-^{k+1}, \bar{u}^k$ is used instead of u^k.

By setting $K=I$, we get an effective algorithm of Model 2 for image denoising directly.

Algorithm 2 Algorithm of Model 2

- Initialization: Set $d^0 = Wf, b^0 = W\mathbf{0}, \lambda_+^0 = \mathbf{0}, \lambda_-^0 = \mathbf{0}, u^0 = f, \bar{u}^0 = f$.
- Iteration: For $k = 0, 1, 2, \ldots$, repeat until a stopping criterion is reached

$$
\begin{aligned}
d^{k+1} &= \text{shrink}\left(\frac{\left(\gamma(W\bar{u}^k + b^k) + t_d^{-1} d^k\right)}{\gamma + t_d^{-1}}, \frac{1}{\gamma + t_d^{-1}}\right),\\
b^{k+1} &= b^k + W\bar{u}^k - d^{k+1},\\
\lambda_+^{k+1} &= \max\{\lambda_+^k + t_\lambda(D(K\bar{u}^k - f) - \tau), 0\},\\
\lambda_-^{k+1} &= \max\{\lambda_-^k + t_\lambda(-D(K\bar{u}^k - f) - \tau), 0\},\\
u^{k+1} &= \left(\mu t_u K^T K + (1 + \gamma t_u) I\right)^{-1} G\\
\bar{u}^{k+1} &= u^k + \theta(u^{k+1} - u^k).
\end{aligned}
$$

- Output: u^{k+1}.

5 Experiments and Comparison

In this section we present the experimental results of the proposed Algorithm $1'$, Algorithm $1''$ and Algorithm 2 with respect to Model 1 and Model 2 on image denoising and image deblurring problems respectively. The proposed methods are compared with some state-of-the-art methods with TV regularization or frame regularization in the follows.

ROF: TV regularization with global constraint as in (3). We use the primal-dual algorithm proposed in [10] to solve it. See [10] for the algorithm details. The fidelity parameter is choosing as $\lambda = 0.03$ for denoising, $\lambda = 10$ for motion deblurring and $\lambda = 0.5$ for Gaussian deblurring in this paper.

TV+Local1: TV regularization with local variance constraint as in Model 1. Remark that this model has been considered in [2], see Sect. 1. We will not follow the algorithm of [2]. That is because the algorithms of TV+Local1 model can be obtained similar as the derivation of Algorithm $1''$ by changing frame analysis operator W as gradient operator ∇, and the frame synthesis W^T as the negative divergence operator ∇^T. However, for image denoising, the algorithm get by this way converges slowly, so we use another more effective algorithm. In this algorithm, we update $\lambda(x)$ and u in two steps. The updating formula of $\lambda(x)$ is chosen to be the same as Algorithm $1'$. When $\lambda(x)$ is fixed, we need to solve the ROF model with variable fidelity parameter $\lambda(x)$:

$$
\min_u \int_\Omega |\nabla u| dx + \frac{\lambda(x)}{2} \|Ku - f\|_2^2. \tag{23}
$$

The derivation of primal-dual algorithm for this problem is the same as the case of ROF model by changing the constant fidelity parameter as variable fidelity parameters. Remark that the initial value of $\lambda(x)$ should not be zero anywhere since $\lambda(x)$ will be the denominator in one of the updating formula. We set the initial $\lambda(x)$ to be a positive constant in our experiments.

TV+Local2: Model in [24] with TV regularization and linear constraint on dictionary decomposition coefficients as in Model 2. The algorithms and parameters setting follow [24] except that in the deblurring case we set $\lambda^0 = \mathbf{10}$ in order to get a smoother image for comparison.

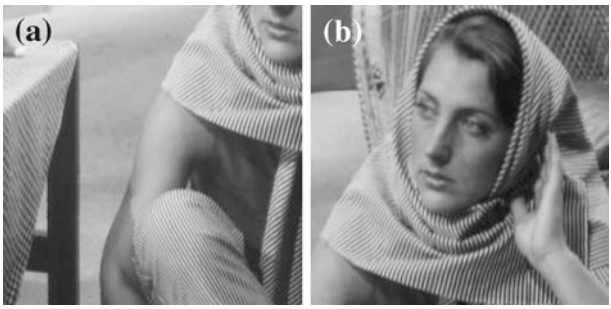

Fig. 1 The true test images with plenty of cartoon regions and texture regions

SA-TV in [13]: The multi-scale method with TV regularization and local constraints as in Model 1. We use the MATLAB source code provided by the authors which can be downloaded from:

http://www.helmholtz-muenchen.de/en/ibb/homepage/yiqiu.dong/Links.html.

It includes the code for image denoising and deblurring with Gaussian kernel and both will be compared with our algorithms. Note that when $\lambda(x)$ is fixed, they use semismooth Newton algorithm to solve a revised version of (23). So in their algorithm, the inner iteration is for this subproblem.

FrameSB in [6]: The image restoration method with frame regularization and global fidelity:

$$\min_u \|Wu\|_1 + \frac{\lambda}{2}\int_\Omega (Ku - f)^2 dx.$$

It is implemented by split Bregman technique. There involves two parameters, one is fidelity coefficient λ, the other is the parameter for the additional term when using split Bregman technique called μ. We choose the parameters by trail and error. The fidelity parameter is choosing as $\lambda = 0.03$ for denoising, $\lambda = 10$ for motion deblurring and $\lambda = 0.5$ for Gaussian deblurring. Wet set $\mu = 0.1$ and frame level=2 in this method.

The first set of test images are two parts of Barbara image with size 256×256 showed in Fig. 1. These images have plenty of texture and cartoon regions and are very adapted to test the restoration models with local constraints, since the aim of local constraints is to recover more textures while smoothing out noise.

In the proposed algorithms, we adopt the piecewise linear B-spline framelet since its effectiveness. It is generated by one low pass filter h_0 and two high pass filters h_1, h_2 which are

$$h_0 = \frac{1}{4}[1, 2, 1],\ h_1 = \frac{\sqrt{2}}{4}[1, 0, -1],\ h_2 = \frac{1}{4}[-1, 2, -1].$$

The frame decomposition level (L) is chosen as 1 or 2 in compromise of quality and computational time. The convolution operator h in Model 1 and TV+Local1 is set as a mean filter with window size 5×5. In the implementation of Model 2 and TV+Local2, we choose the dictionary $\mathcal{D}$ as in [24]: the dictionary received by the full wavelet packet decomposition up to level four in which the wavelet filter is set as "sym8" (applied by MATLAB using the freeware Wavelab850 which can be downloaded from http://www-stat.stanford.edu/wavelab).

The peak signal-to-noise ratio (PSNR) is adopted to measure the quality of the recovered images which is defined as:

$$PSNR(u,\tilde{u}) = 10\log 10\left(\frac{255^2}{\frac{1}{mn}\|u-\tilde{u}\|_2^2}\right)$$

where u is the restored image and $\tilde{u}$ is the true image, m and n denote the size of the image. The stopping criterion is that the relative error between the successive iterate of the restored image should satisfy the following inequality:

$$\frac{\|u^{k+1}-u^k\|_2}{\|u^{k+1}\|_2} < \epsilon.$$

We set $\epsilon = 10^{-4}$ for image denoising problems and $\epsilon = 0.5 * 10^{-4}$ for image deblurring problems.

All the experiments are performed under Windows 7 and MATLAB v7.4 with Intel Core i5 M450 CPU and 2GB memory.

5.1 Image Denoising

For image denoising, we add Gaussian white noise with zero mean and standard deviation $\sigma = 20$ on Fig. 1a and get the noisy image in Fig. 2a. Then we compare the denoising performance of seven methods including ROF, TV+Local1, TV+Local2, FrameSB, SA-TV and the proposed Algorithm $1'$ and Algorithm 2 on this noisy image. In the following, we list all the parameters involved in the proposed algorithms:

Algorithm $1'$: $\lambda^0 = \mathbf{0}, \rho = 0.01, \gamma = 0.5, \sigma = 20, \bar{\sigma}^2 = 2.5\sigma^2, L = 1.$
Algorithm 2: $\lambda^0 = \mathbf{0}, t_u = 1, t_\lambda = 0.1, t_d = 10, \mu = 0.06, \theta = 1, \gamma = 0.5, \tau = 75, L = 1.$

By ROF method in which global constraint is used, textures are almost lost while smoothing out noise, see Fig. 2b. It is obvious that textures can be better preserved by models with local constraints and FrameSB, see Fig. 2c–g. After a careful comparison of Fig. 2c, d with Fig. 2e–g, we find that the frame based models can recover more textures and has less staircase effect in the cartoon regions than TV based methods. In terms of PSNR, the proposed Algorithm $1'$ has a higher PSNR of 0.6 dB than TV+Local1, and the proposed Algorithm 2 has a higher PSNR of 0.8 dB than TV+Local2. Moreover, the proposed methods with local constraints can recover more textures than the FrameSB method with global constraint. The PSNR of the Algorithm $1'$ and Algorithm 2 is higher than FrameSB about 0.8 dB and 0.5 dB respectively. The iterations and computational time of each algorithm are also reported. We observe that the operation of dictionary is time consuming, and tight frame consumes more time than TV in each iteration. All the algorithms with local constraints converges in less iterations than the ROF model with global constraint. Among all TV+Local1 takes the shortest time. In a whole, the proposed algorithms are efficient which converge to satisfactory results in about 20 s.

Figure 3a–d show the value of $\lambda(x)$ or $D^T(\lambda_+)(x)$ correspond to Fig. 2c, d, f, g respectively. Since the image of $D^T(\lambda_-)(x)$ seems similar with $D^T(\lambda_+)(x)$, we omit them. We observe that Fig. 3a, c are similar, while Fig. 3b, d are similar. This fact shows something different behavior of the two types of local constraints in Model 1 and Model 2. Since a convolution kernel h is used in Model 1, the output $\lambda(x)$ seems smooth. However, a careful observation tells us in every case, $|\lambda(x)|$ and $|D^T(\lambda_+)(x)|$ are large in the texture regions and relatively

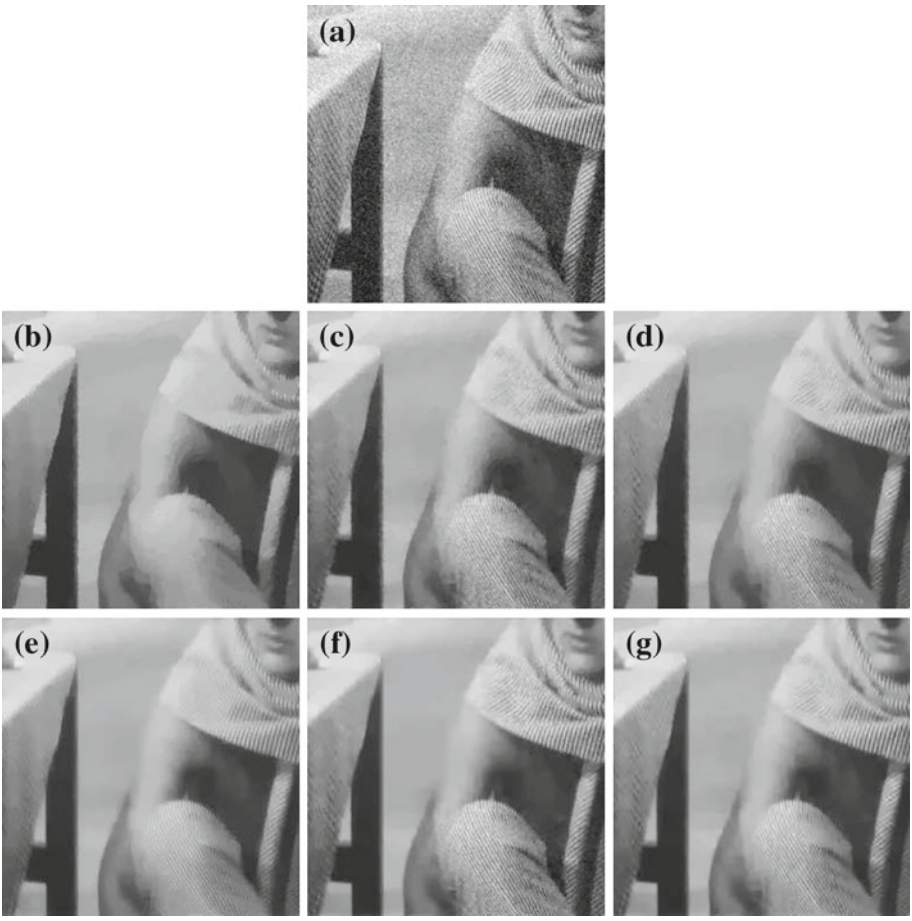

Fig. 2 Image denoising. **a** Image corrupted by Gaussian white noise with mean zero and standard deviation 20; **b** Result of ROF, PSNR = 24.45 dB, iteration = 348, T = 4.9 s; **c** Result of TV+Local1, PSNR = 26.75 dB, iteration = 92, T = 2.5 s; **d** Result of TV+Local2, PSNR = 26.25 dB, iteration = 97, T = 19.3 s; **e** Result of FrameSB, PSNR = 26.50 dB, iteration = 37, T = 12.7 s; **f** Result of Algorithm 1′, PSNR = 27.37 dB, iteration = 174, T = 22.6 s; **g** Result of Algorithm 2, PSNR = 27.05 dB, iteration = 74, T = 23.2 s

small in the cartoon regions. Hence more fidelity is favored in the texture regions such that the textures are better recovered by the models with local constraints than with global constraint under the assumption that the same regularization technique is used. Actually, from the denoising comparison on texture images, we also find that with the same type of fidelity term, frame based regularization works better than TV regularization. We also remark that comparing Fig. 3a, c, we find that Fig. 3c detects textures regions more accurate than Fig. 3a.

In Fig. 4, we compare the performance of the six methods including ROF, FrameSB, TV+Local1, TV+Local2, the proposed Algorithm 1′ for Model 1 and Algorithm 2 for Model 2. We run each algorithm 200 iterations. Figure 4a shows that the proposed Algorithm 1′ and Algorithm 2 achieve higher PSNR than other algorithms after about 50 iterations, meanwhile Algorithm 1′ is slightly higher than Algorithm 2. ROF has the lowest PSNR among all. In the first a few iterations of Algorithm 1′, there is an oscillation of PSNR. But after that, the algorithm seems stable and converges to satisfactory result.

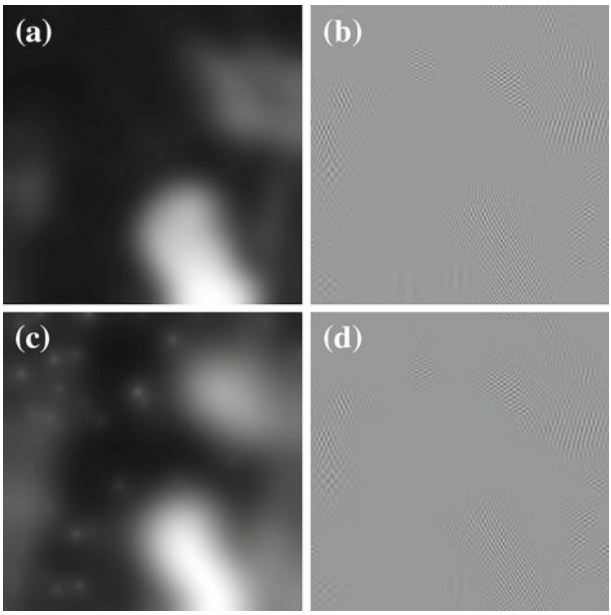

Fig. 3 Final values of $\lambda(x)$ or $D^T(\lambda_+)(x)$. **a** $\lambda(x)$ corresponds to Fig. 1c; **b** $D^T(\lambda_+)(x)$ corresponds to Fig. 1d; **c** $\lambda(x)$ corresponds to Fig. 1f; **d** $D^T(\lambda_+)(x)$ corresponds to Fig. 1g

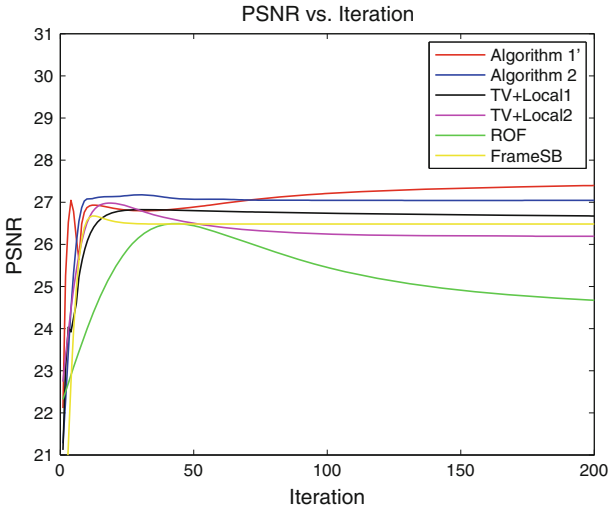

Fig. 4 Image denoising: comparison of PSNR of ROF, TV+Local1, TV+Local2, FrameSB and the proposed Algorithm $1'$ and Algorithm 2, all run 200 iterations

In Fig. 5, we display the denoising result of Fig. 2a with SA-TV method in [13]. Remark that we use all the default parameters in the source code except that the initial λ^0 is tuned to achieve the optimal result. Finally, we choose $\lambda^0 = 3.6$. SA-TV achieves PSNR of 26.55 dB which is about 0.5 dB lower than our results with frame regularization in Fig. 2f, g.

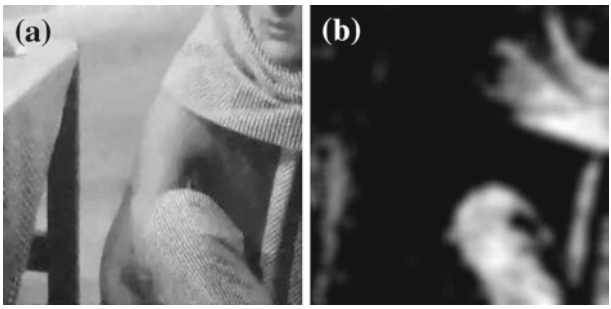

Fig. 5 The denoising result of SA-TV algorithm. **a** Denoising result, PSNR = 26.55 dB, outer iteration = 1, T = 66.4 s; **b** Final value of $\lambda(x)$

5.2 Image Deblurring

In this subsection, we test the algorithms on image deblurring problems. We test both motion blur and Gaussian blur with white Gaussian noise.

5.2.1 Motion Blur Case

The degraded image in Fig. 6a is generated like this: first apply a motion blur on the true image Fig. 1b, then add Gaussian noise with zero mean and standard deviation $\sigma = 1$ on it. The motion blur kernel is generated by the MATLAB routine "fspecial" with length of 30 pixels and angle 45 degree. In deblurring case, we assume periodic boundary conditions since fast Fourier transform (FFT) will be used to solve u^{k+1} in both Algorithm 1″ and Algorithm 2. All the parameters involved in the proposed algorithms are:

Algorithm 1″: $\lambda^0 = \mathbf{10}$, $\rho = 1, \gamma_1 = 0.1, \gamma_2 = 1, \sigma = 1, \tilde{\sigma}^2 = 1.3\sigma^2, L = 1$.

Algorithm 2: $\lambda^0 = \mathbf{0}, t_u = 1, t_\lambda = 0.1, t_d = 10, \mu = 20, \theta = 1, \gamma = 0.5, \sigma = 1, \tau = 2\sigma, L = 1$.

Figure 6b–f display the result of six methods include ROF, TV+Local1, TV+Local2, FrameSB and the proposed two models with the specified Algorithm 1″ and Algorithm 2. In Fig. 6b, we find that ROF removes so many textures, while textures are better preserved by the other five methods. With TV regularization technique, there can be seen some staircase effects occur on the faces and the left side cartoon regions in Fig. 6b–d. Figure 6f–g give the results of frame based algorithms which preserve many textures with less staircase effects in cartoon regions. Figure 6e shows that the result of FrameSB suffers less staircase effect than TV based method, however, the textures is over smoothed compared with Fig. 6f, g. In terms of PSNR, methods with local constraints are higher than ROF method of 1.4–3.0 dB. With frame regularization, the proposed methods with local constraints have higher PSNR than FrameSB with global constraint about 0.7 dB. In a whole, the proposed algorithms have the highest PSNRs. The iterations and computational time are also reported. In the deblurring case, models with local constraints converges at about 500 iterations which are slower than ROF method with 189 iterations and FrameSB with 126 iterations. However, the algorithms are still effective since about two-three minutes are needed to get satisfactory results.

The values of $\lambda(x)$ or $D^T(\lambda_+)(x)$ correspond to Fig. 6c, d, f, g are showed in Fig. 7. Again, we omit the image of $D^T(\lambda_-)(x)$ since it is similar to $D^T(\lambda_+)(x)$. We observe that Fig. 7a, c are similar in which local variance constraints are used, while Fig. 7b, d are similar in which linear constraints of dictionary decomposition coefficients are used. A careful observation

Fig. 6 Image deblurring. **a** Image corrupted by motion blur and Gaussian white noise of standard deviation 1; **b** Result of ROF, PSNR = 24.77 dB, iteration = 189, T = 4.6 s; **c** Result of TV+Local1, PSNR = 26.17 dB, iteration = 470, T = 37.1 s; **d** Result of TV+Local2, PSNR = 26.61 dB, iteration = 512, T = 139.5 s; **e** Result of FrameSB, PSNR = 26.23 dB, iteration = 126, T = 46.6 s; **f** Result of Algorithm 1″, PSNR = 26.94 dB, iteration = 726, T = 106.8 s; **g** Result of Algorithm 2, PSNR = 27.08 dB, iteration = 503, T = 183.4 s;

shows that $|\lambda(x)|$ and $|D^T(\lambda_+)(x)|$ are large in the texture regions and relatively small in the cartoon regions. Hence the textures are better recovered by the models with local constraints than the models with global constraint under the condition that the the same regularization term is used.

The performance of the six methods are further compared in Fig. 8. We run each algorithm 500 iterations. We observe in Fig. 8a that the proposed Algorithm 1″ and Algorithm 2 achieve higher PSNR than other algorithms, and Algorithm 2 has the highest PSNR among all after about 200 iterations. ROF has the lowest PSNR among all.

5.2.2 Gaussian Blur Case

In the case of Gaussian blur, we compare the proposed methods with ROF, SA-TV and FrameSB in Fig. 9. The test image in Fig. 9a is generated like this: first apply a Gaussian blur

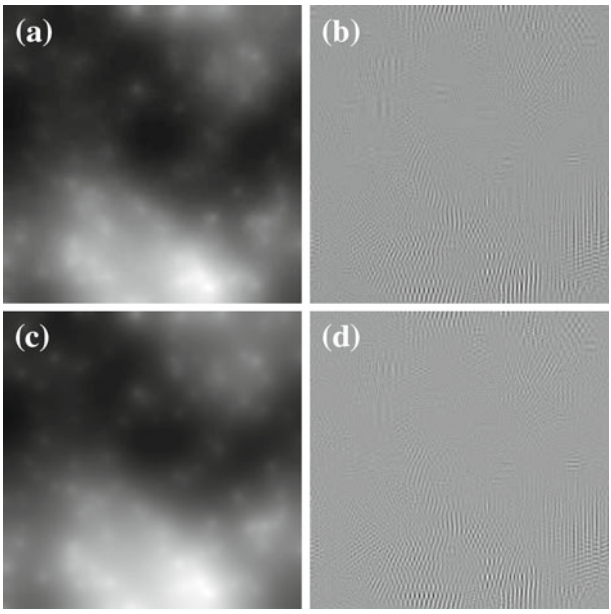

Fig. 7 Final values of $\lambda(x)$ or $D^T(\lambda_+)(x)$. **a** $\lambda(x)$ corresponds to Fig. 6c; **b** $D^T(\lambda_+)(x)$ corresponds to Fig. 6d; **c** $\lambda(x)$ corresponds to Fig. 6f; **d** $D^T(\lambda_+)(x)$ corresponds to Fig. 6g

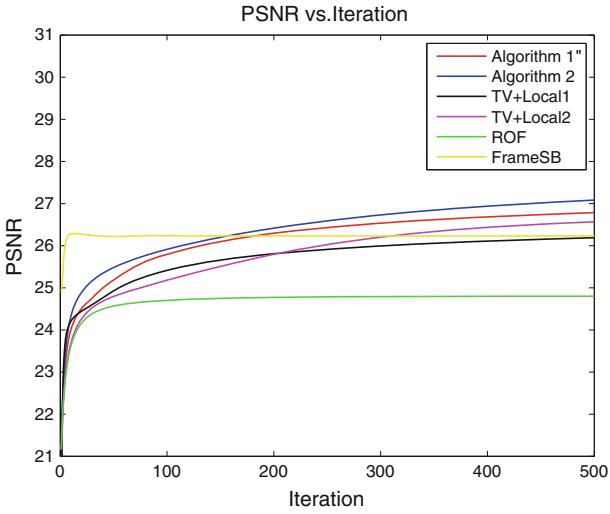

Fig. 8 Motion deblurring: comparison of PSNR of ROF, TV+Local1, TV+Local2, FrameSB and the proposed Algorithm $1''$ and 2, all run 500 iterations

on the true image Fig. 1b, then add Gaussian noise with zero mean and standard deviation $\sigma = 5$ on it. The Gaussian blur kernel is generated by the MATLAB routine "fspecial" with window size 9×9 and standard deviation 1. All the default parameters in the source code of [13] are used for SA-TV. All the parameters involved in the proposed algorithms are:

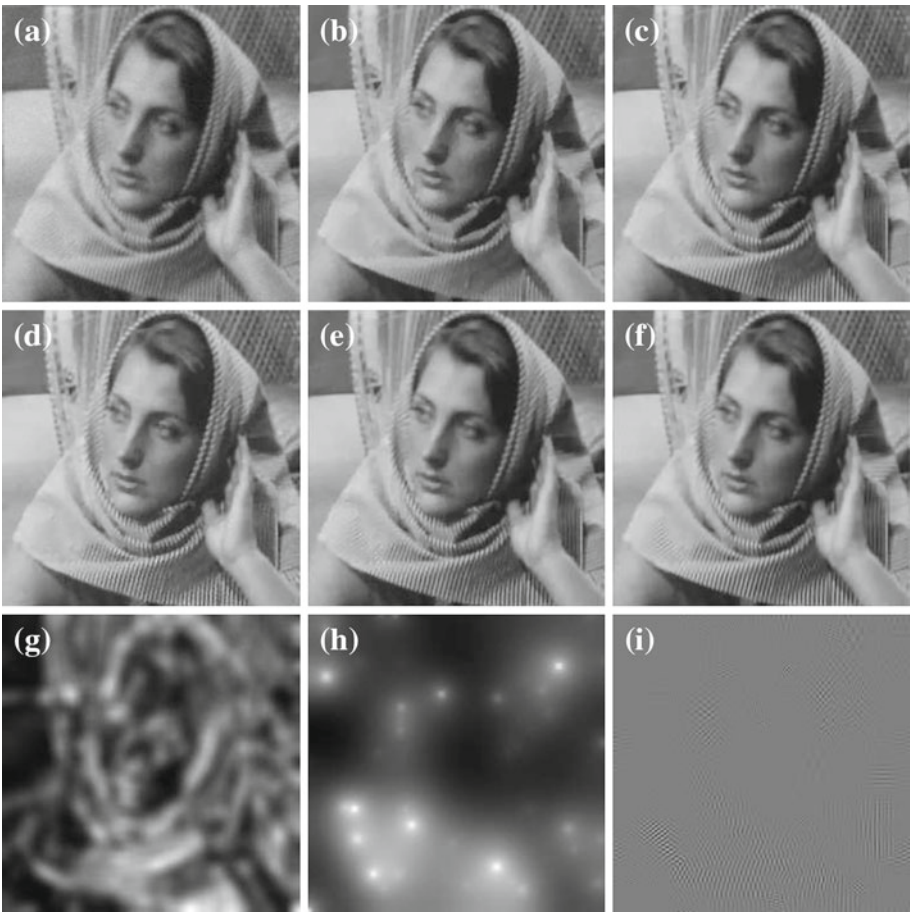

Fig. 9 Image deblurring. **a** Image corrupted by Gaussian blur and Gaussian white noise of standard deviation $\sigma = 5$; **b** Result of ROF, PSNR = 25.27 dB, iteration = 96, T = 2.5 s; **c** Result of FrameSB, PSNR = 27.19 dB, iteration = 135, T = 47.5 s; **d** Result of SA-TV, PSNR = 27.53 dB, out iteration = 6, T = 1942.5 s; **e** Result of Algorithm 1″, PSNR = 27.95 dB, iteration = 603, T = 156.7 s; **f** Result of Algorithm 2, PSNR = 28.11 dB, iteration = 177, T = 82.7 s; **g** Final value of $\lambda(x)$ corresponds to **d**; **h** Final value of $\lambda(x)$ corresponds to **e**; **i** Final value of $D^T(\lambda_+)(x)$ corresponds to **f**

Algorithm 1″: $\lambda^0 = \mathbf{0.3}$, $\rho = 1$, $\gamma_1 = 0.1$, $\gamma_2 = 0.1$, $\sigma = 5$, $\bar{\sigma}^2 = 2\sigma^2$, $L = 2$.
Algorithm 2: $\lambda^0 = \mathbf{0}$, $t_u = 1$, $t_\lambda = 0.1$, $t_d = 10$, $\mu = 1.5$, $\theta = 1$, $\gamma = 0.5$, $\sigma = 5$, $\tau = 3\sigma$, $L = 2$.

Figure 9b is the result of ROF method. Most of the textures are lost. With frame based regularization, FrameSB recovers more textures, see Fig. 9c. It is obvious that the methods with local constraints can better recover textures than ROF, see the second row of Fig. 9 for the results of SA-TV algorithm, Algorithm 1″ and Algorithm 2. With a careful look at Fig. 9c–f, we find that our algorithms recovers textures better than FrameSB and SA-TV. For example, the textures on the left bottom part of Barbara's scarf are almost smoothed out by FrameSB and SA-TV, while the proposed algorithms keeps some of the textures. The final value of $\lambda(x)$ or $D^T(\lambda^+)(x)$ are displayed in the third row, Fig. 9g–i. The appearance

Table 1 Comparison of PSNR (dB): Gaussian noise case

Image	ROF	FrameSB	TV+Local1	TV+Local2	Model 1	Model 2
Couple	27.91	28.07	28.10	28.37	29.10	29.38
Boat	28.37	28.46	28.62	28.79	29.35	29.72
Lena	30.42	30.65	28.20	30.88	31.25	31.53

Table 2 Comparison of PSNR (dB): motion blur case

Image	ROF	FrameSB	TV+Local1	TV+Local2	Model 1	Model 2
Couple	27.35	28.14	28.52	28.42	28.66	28.89
Boat	27.96	28.71	28.78	28.98	29.17	29.44
Lena	31.38	31.44	31.42	31.93	32.19	32.39

Table 3 Comparison of PSNR (dB): Gaussian blur case

Image	ROF	FrameSB	TV+Local1	TV+Local2	Model 1	Model 2
Couple	29.43	29.62	30.30	30.32	30.53	30.88
Boat	29.83	29.98	30.66	30.65	30.81	31.15
Lena	32.89	33.05	33.42	33.69	33.76	34.00

seems greatly different, however, the common property is that the absolute values are bigger in texture regions than cartoon regions. For quantitative evaluation of the algorithms, we reported the PSNR, iteration and the computational time. In terms of PSNR, the proposed algorithms are about 0.7–0.9 dB higher than FrameSB, and about 0.4–0.6 dB higher than SA-TV. We report only the outer iteration of SA-TV. Remark that in each outer iteration, a maximum inner iteration is set as 50. SA-TV takes about half an hour to converge which is far more computational expensive than our algorithms which take less than three minutes to get satisfactory results.

To further demonstrate the effectiveness of our proposed methods, we present more results and comparisons in Tables 1, 2 and 3. The three test images are downloaded from the website: http://www.cs.tut.fi/foi/GCF-BM3D/. The three degradation cases in the Tables are generated the same as in Sects. 5.1, 5.2.1 and 5.2.2. We find that the proposed Model 1 and Model 2 have higher performance than the other TV based models. Moreover, the proposed Model 2 has the highest PSNR among all.

6 Conclusions

Two models with tight frame regularization and two types of local constraints are studied in this paper. For each model, we design effective numerical algorithms based on SB and DAL methods, such that the original problem can be split into several simple subproblems with closed-form solutions. The proposed models have better performance than TV regularization based models by reducing staircase effect in the cartoon regions and preserving more textures. The proposed frame based methods with local constraints also outperforms the frame based

method with global constraint. Numerically the proposed algorithms are easy to implement and efficient. As a byproduct, the algorithm used in this paper for TV+Local1 seems more brief than the counterpart in existing literatures. The future work is to extend the models and algorithms for image restoration problems with multiplicative noise and blur, which aims to recover more textures and improve image quality.

References

1. Afonso, M.V., Bioucas-Dias, J.M., Figueiredo, M.A.T.: Fast image recovery using variable splitting and constrained optimization. IEEE Trans. Image Process. **19**(9), 2345–2356 (2010)
2. Almansa, A., Ballester, C., Caselles, V., Haro, G.: A TV based restoration model with local constraints. J. Sci. Comput. **34**(3), 209–236 (2008)
3. Aubert, G., Kornprobst, P.: Mathematical Problems in Image Processing: Partial Differential Equations and the Calculus of Variations, vol. 147. Springer, New York (2006)
4. Bertalmio, M., Caselles, V., Rougé, B., Solé, A.: TV based image restoration with local constraints. J. Sci. Comput. **19**(1), 95–122 (2003)
5. Cai. J.-F., Dong, B., Osher, S., Shen, Z.: Image restoration: total variation, wavelet frames, and beyond. J. Am. Math. Soc. (to appear) (2012)
6. Cai, J.-F., Osher, S., Shen, Z.: Split bregman methods and frame based image restoration. Multiscale Model. Simul. **8**(2), 337–369 (2009)
7. Cai, J.-F., Shen, Z.: Framelet based deconvolution. J. Comput. Math. **28**(3), 289–308 (2010)
8. Chambolle, A.: An algorithm for total variation minimization and applications. J. Math. Imaging Vis. **20**(1), 89–97 (2004)
9. Chambolle, A., Lions, P.L.: Image recovery via total variation minimization and related problems. Numer. Math. **76**(2), 167–188 (1997)
10. Chambolle, A., Pock, T.: A first-order primal-dual algorithm for convex problems with applications to imaging. J. Math. Imaging Vis. **40**(1), 120–145 (2011)
11. Dong, B., Shen, Z.: MRA-Based Wavelet Frames and Applications. UCLA CAM reports 10–69 (2010)
12. Dong, B., Zhang, Y.: An efficient algorithm for l_0 minimization in wavelet frame based image restoration. Technical report, UCLA CAM reports, cam11-66 (2011)
13. Dong, Y., Hintermíźller, M., Camacho, M.R.: Automated regularization parameter selection in multi-scale total variation models for image restoration. J. Math. Imaging Vis. **40**(1), 82–104 (2011)
14. Eckstein, J., Bertsekas, D.P.: On the douglasałrachford splitting method and the proximal point algorithm for maximal monotone operators. Math. Program. **55**(1), 293–318 (1992)
15. Faurre, P.: Analyse numéique. Notes d'optimisation. École Polytechnique. Ed. Ellipses (1988)
16. Gabay, D.: Applications of the method of multipliers to variational inequalities. In: Fortin, M., Glowinski, R. (eds.) Studies in mathematics and its applications, chapter 6, pp. 299–331. North-Holland, Amsterdam (1983)
17. Gilboa, G., Sochen, N., Zeevi, Y.Y.: Variational denoising of partly textured images by spatially varying constraints. IEEE Trans. Image Process. **15**(8), 2281–2289 (2006)
18. Goldstein, T., Osher, S.: The split bregman method for l1 regularized problems. SIAM J. Imaging Sci. **2**(2), 323–343 (2009)
19. Hahn, J., Wu, C., Tai, X.C.: Augmented lagrangian method for generalized tv-stokes model. J. Sci. Comput. **50**(2), 235–264 (2012)
20. Hintermüller, M., Rincon-Camacho, M.M.: Expected absolute value estimators for a spatially adapted regularization parameter choice rule in l1-tv-based image restoration. Inverse Probl. **26**(8), 85005–85034 (2010)
21. Iusem, A.N.: Augmented lagrangian methods and proximal point methods for convex optimization. Investigación Operativa **8**, 11–49 (1999)
22. Li, F., Ng, M.K., Shen, C.: Multiplicative noise removal with spatially varying regularization parameters. SIAM J. Imaging Sci. **3**(1), 1–22 (2010)
23. Lintner, S., Malgouyres, F.: Solving a variational image restoration model which involves l^∞ constraints. Inverse Probl. **20**, 815–831 (2004)
24. Ma, L., Mosian, L., Yu, J., Zeng, T.: Stable method in solving total variation dictionay model with l^∞ constraints. HongKong Baptist University (HKBU), Technical report (2011)
25. Malgouyres, F.: Mathematical analysis of a model which combines total variation and wavelet for image restoration. J. Inf. process. **2**(1), 1–10 (2002)

26. Rockafellar, R.T.: Monotone operators and the proximal point algorithm. SIAM J. Control Optim. **14**(5), 877–898 (1976)
27. Rudin, L.I., Osher, S.: Total variation based image restoration with free local constraints. In: Image Processing, 1994. Proceedings. ICIP-94., IEEE International Conference, 1, pp. 31–35. IEEE (1994)
28. Rudin, L.I., Osher, S., Fatemi, E.: Nonlinear total variation based noise removal algorithms. Physica D: Nonlinear Phenomena **60**, 259–268 (1992)
29. Setzer, S.: Operator splittings, bregman methods and frame shrinkage in image processing. Int. J. Comput. Vis. **92**(3), 265–280 (2011)
30. Setzer, S., Steidl, G., Teuber, T.: Deblurring poissonian images by split bregman techniques. J. Vis. Commun. Image Represent. **21**(3), 193–199 (2010)
31. Strong, D., Chan, T.: Edge-preserving and scale-dependent properties of total variation regularization. Inverse Probl. **19**(6), S165–S187 (2003)
32. Tai, X.C., Hahn, J., Chung, G.J.: A fast algorithm for euler's elastica model using augmented lagrangian method. SIAM J. Imaging Sci. **4**, 313–344 (2011)
33. Wu, C., Tai, X.C.: Augmented lagrangian method, dual methods, and split bregman iteration for rof, vectorial tv, and high order models. SIAM J. Imaging Sci. **3**(3), 300–339 (2010)
34. Zeng, T., Ng, K.: On the total variation dictionary model. IEEE Trans. Image Process. **19**(3), 821–825 (2010)